PAPER

Scalar gravitational wave signals from core collapse in massive scalar–tensor gravity with triple-scalar interactions

View the article online for updates and enhancements.

Scalar gravitational wave signals from core collapse in massive scalar–tensor gravity with triple-scalar interactions

Da Huang[1,2,3,*] , **Chao-Qiang Geng**[2,3,4,5]
and Hao-Jui Kuan[4,6]

[1] National Astronomical Observatories, Chinese Academy of Sciences, Beijing 100101, People's Republic of China
[2] School of Fundamental Physics and Mathematical Sciences, Hanzhou Institute for Advanced Study, UCAS, Hanzhou 310024, People's Republic of China
[3] International Centre for Theoretical Physics Asia-Pacific, Beijing/Hanzhou, People's Republic of China
[4] Department of Physics, National Tsing Hua University, Hsinchu 300, Taiwan, Republic of China
[5] Synergetic Innovation Center for Quantum Effects and Applications (SICQEA), Hunan Normal University, Changsha 410081, People's Republic of China
[6] Theoretical Astrophysics, IAAT, University of Tubingen, Tubingen, Germany

E-mail: dahuang@bao.ac.cn, geng@phys.nthu.edu.tw and guanhauwzray@gmail.com

Abstract

The spontaneous scalarization during the stellar core collapse in the massive scalar–tensor theories of gravity introduces extra polarizations (on top of the plus and cross modes) in gravitational waves, whose amplitudes are determined by several model parameters. Observations of such scalarization-induced gravitational waveforms therefore offer valuable probes into these theories of gravity. Considering a triple-scalar interactions in such theories, we find that the self-coupling effects suppress the magnitude of the scalarization and thus reduce the amplitude of the associated gravitational wave signals. In addition, the self-interacting effects in the gravitational waveform are shown to be negligible due to the dispersion throughout the astrophysically distant propagation. As a consequence, the gravitational waves observed on the Earth feature the characteristic inverse-chirp pattern. Although not with the on-going ground-based detectors, we illustrate that the scalarization-induced gravitational waves may be detectable at a signal-to-noise ratio level of $\mathcal{O}(100)$ with future detectors, such as Einstein Telescope and Cosmic Explorer.

*Author to whom any correspondence should be addressed.

(Some figures may appear in colour only in the online journal)

1. Introduction

Even though general relativity (GR) has so far withstood all experimental tests [1–4], many theoretical considerations signal the need of alternative theories of gravity beyond the GR, e.g. the non-renormalizability of GR [5], and numerous astrophysical and cosmological observations [6] (see reference [2] for a recent review). An abundance of modified theories of gravity have been constructed to extend GR to overcome the aforementioned obstacles. Among them, the most widely explored one may be the scalar–tensor (ST) theories of gravity [7–9] in which the gravitational interaction is mediated not only by the metric tensor but also by an additional scalar field.

Due to its simplicity and well-posedness [10, 11], ST theories have been subjected to a wide range of experimental tests [12–18], while most are performed in the weak-field regime (mainly in the Solar System) [19–22]. Nonetheless, with appropriate ST parameters and strong enough spacetime curvature (see, e.g. [23]), strongly-scalarized neutron star (NS) solutions are energetically favored over the ordinary weakly-scalarized ones [24]. The ST gravity therefore allows a nonperturbative strong-field phenomenon known as the *spontaneous scalarization* [25, 26] in NSs. Such phenomenon induces a non-vanishing dipole charge of the scalar field, which is stringently constrained by observations of binary pulsar timings [27–30]. However, in massive ST theories, the introduction of the scalar mass $\mu \gtrsim 10^{-15}$ eV effectively weakens these experimental constraints on the parameters [31–33] so that the theory leaves more room for parameters that can lead to strongly-scalarized NS solutions. In addition, the recent detections of gravitational waves (GWs) have opened a novel window to limit the ST gravity, which has already set severe constraints on the possible models [4, 34–36]. A further constraint on the ST gravity arises from the equivalence between the Jordan and Einstein frames [37, 38].

As the evolutionary endpoint of a star, the core collapse to form an NS or a black hole (BH) constitutes another testbed for the strong-field dynamics of the ST gravities [2, 31, 39]. In particular, if a scalarized proto-NS forms during the collapse, the sharp transition from the weakly-scalarized star configuration into the strongly-scalarized state generates scalar- or monopole-polarized GWs, which is a critical feature of the ST gravity that is absent in GR. Early studies on the spontaneous scalarization and scalar GW production were concentrated on the massless ST gravity [40–43]. In order to evade the strong experimental constraints listed above, references [44, 45] initiated a line of studies on the core collapse in the massive ST theories. In references [46, 47], the theory was further extended to the case with scalar self-interactions which generically suppressed the degree of the scalarization and the amplitude of the scalar GW radiation.

However, previous studies only focused on the effects of the even-power scalar self-interactions [46, 47] defined in the Einstein frame. Odd-power scalar self-interactions have not been explored yet. Given the importance of the stellar collapse in testing ST gravity by, e.g. scalarization-induced GW signals that are potentially measurable with the ground-based GW detectors, any ST model warrants further investigations. In the present paper, we study the core collapse and the monopole GW radiations in the massive ST theories, including the simplest odd-power scalar self-interaction in the Einstein frame, viz the triple-scalar coupling effects.

In order to ensure the stability of the theory, we take the absolute value of the triple-scalar interaction in the scalar potential. The influence of this scalar interaction on the spontaneous scalarization and the scalar GW production during the core collapse is explored by considering two particular collapse progenitors, which have been treated in the massless [43] and massive [37, 44] ST theories. One of them leads to an NS remnant and the other settles to a BH. We also consider the impact of the triple-scalar coupling on the astrophysically long-distance dispersive propagation of the scalar GWs in our Galaxy, which generically leads to the inverse-chirp feature of the GW signals detected on the Earth. Finally, we assess the detectability of the possible scalar GW signals in the on-going and up-coming ground-based GW detectors by computing the corresponding signal-to-noise ratios (SNRs).

The paper is organized as follows. In section 2, we present a brief introduction to the self-interacting massive ST theories and specify the triple-scalar interaction that is considered. The equation of state obeyed by the nuclear matter during the stellar core collapse is introduced as well. In section 3, the setup of our simulations is detailed. We also show the numerical results of the core collapses with a specific attention paid to the self-interaction effects on the scalar dynamics and the associated GW waveforms. Section 4 is devoted to studying the influence of the triple-scalar coupling on the large-distance propagation of the scalar GWs and the detectability of these GW signals. Finally, we offer our conclusions and some further discussions in section 5.

2. Formalism

In the ST theories of gravity, the gravitational fields are augmented by an extra scalar field $\phi(x)$ in addition to the spacetime metric tensor $g_{\mu\nu}(x)$. In this work, we are interested in the ST gravity first proposed by Bergmann [48] and Wagoner [49], in which (i) the single scalar field non-minimally couples to the metric tensor; (ii) the theory is diffeomorphism invariant; (iii) the variation of the action gives rise to second order field equations; and (iv) the weak equivalence principle is satisfied [in the Jordan (physical) frame, see below]. In the literature, the most general action of this class of theories can be written as [2]

$$S_{\mathrm{J}} = \int \mathrm{d}^4 x \frac{\sqrt{-g}}{16\pi} \left(F(\phi)R - \frac{\omega(\phi)}{\phi} g^{\mu\nu}\partial_\mu\phi\partial_\nu\phi - U(\phi) \right) + S_m[\psi_m, g_{\mu\nu}], \quad (1)$$

in natural units $G = c = 1$, where $F(\phi)$, $\omega(\phi)$ and $U(\phi)$ are continuous and differentiable functions of the scalar field ϕ with the existence of second-order derivatives, and S_m represents the action of ordinary matter fields that are collectively denoted by ψ_m. Note that matter fields couple to the gravity sector only through the (physical) metric tensor $g_{\mu\nu}$ without any dependence on ϕ, so that the weak equivalence principle holds.

One can also formulate the same theory in the so-called Einstein's frame, which relates to the Jordan frame via a Weyl transformation,

$$\bar{g}_{\mu\nu} \equiv g_{\mu\nu}/F(\varphi), \quad (2)$$

and a redefinition of the scalar field,

$$\frac{\mathrm{d}\varphi}{\mathrm{d}\phi} := \pm \sqrt{\frac{3(F_{,\phi})^2}{4F^2} + \frac{\omega}{2\phi F}}. \quad (3)$$

The action equation (1) reads

$$S_{\rm E} = \int {\rm d}^4 x \frac{\sqrt{-\bar{g}}}{16\pi} \left(\bar{R} - 2\bar{g}^{\mu\nu} \partial_\mu \varphi \partial_\nu \varphi - 4V(\varphi) \right) + S_m[\psi_m, \bar{g}_{\mu\nu}/F(\varphi)], \qquad (4)$$

in the Einstein frame, where the scalar potential $V(\varphi)$ is related to the one in the Jordan frame through [37, 38]

$$V(\varphi) := U(\phi)/(4F^2). \qquad (5)$$

One can see that the ST theory in the Einstein frame is specified by the scalar potential $V(\varphi)$ and the conformal factor $F(\varphi)$. The latter controls the coupling between the scalar field φ and ordinary matters. In the present article, we adopt the following parametrization of the conformal factor [12, 13, 26]

$$\ln F(\varphi) \equiv -2\alpha_0(\varphi - \varphi_0) - \beta_0(\varphi - \varphi_0)^2, \qquad (6)$$

which is nothing but merely the Taylor expansion [26]. Note that the two free dimensionless parameters α_0 and β_0 is not only sufficient to determine the first-order post-Newtonian effects, but also contribute to higher post-Newtonian orders. Moreover, φ_0 denotes the asymptotic value of the scalar field at spatial infinity.

Massive scalar fields with a triple-scalar self-interaction have the scalar potential given by

$$V(\varphi) = \frac{\mu^2}{2\hbar^2}(\varphi^2 + \lambda|\varphi|^3), \qquad (7)$$

where λ is assumed to be positive and the absolute value is taken in the scalar self-interaction term in order to guarantee the semi-positivity and stability of the potential. Thus, the asymptotic value of φ should naturally be $\varphi_0 = 0$, which is the absolute minimum of this potential. Moreover, the scalar field mass is fixed to be $\mu = 10^{-14}$ eV, which not only alleviates the strong constraints from binary pulsars and weak field tests of GR [31, 32], but also allows the propagating monopole GW signals to be detectable [44, 45] in the LIGO/Virgo sensitivity window. For the later convenience, we also define a characteristic frequency

$$f_* = \frac{\omega_*}{2\pi} \equiv \mu/(2\pi\hbar) \simeq 2.42 \text{ Hz}, \qquad (8)$$

which is associated with the scalar mass.

2.1. Spherical collapse

The stellar core collapse into a compact object such as NS and BH marks the end-point of a massive star with the zero-age main sequence (ZAMS) mass in the range of $10M_\odot \lesssim M_{\rm ZAMS} \lesssim 130M_\odot$ [51–53] with $M_\odot$ denoting the solar mass. At the end of the nuclear burning phase of a star, the nuclear matter thermal pressure and the electrons' degenerate pressure can no longer balance the huge gravitational attracting force [54], leading to a sudden radial compression of the matter. The collapse increases the central (baryon) mass density up to the nuclear density $\rho_{\rm nuc} \simeq 2 \times 10^{14}$ g cm^{-3} [55] beyond which the compression is halted and the inner core bounces due to the repulsive force

stemmed from the stiffening of the nuclear matter. The core bounce launches a hydrodynamic shockwave outwards and a core-collapse supernova explosion (CCSNe) may then be generated[7].

We assume a spherically symmetric ansatz for which the line element is given by [50]

$$ds^2 = -F\alpha^2 \, dt^2 + FX^2 \, dr^2 + r^2(d\theta^2 + \sin^2\theta \, d\phi^2), \tag{9}$$

where X and α are functions of the coordinates r and t. The stellar matter is modeled as the a perfect fluid whose energy–momentum tensor reads [61]

$$T_{\mu\nu} = (\rho + \rho\epsilon + P)u_\mu u_\nu + Pg_{\mu\nu}, \tag{10}$$

in the Jordan frame, where ρ, P, ϵ, and u^μ represent the baryon density, pressure, internal energy and the four-velocity of the nuclear matter, respectively. In order to account for the stiffness of the nuclear matter and thermal effects experienced by the shock, we would like to follow references [43–45] to apply the hybrid equation of state (EOS) [55, 62, 63]

$$P = P_c + P_{th}, \qquad \epsilon = \epsilon_c + \epsilon_{th}, \tag{11}$$

which comprise the cold parts (P_c, ϵ_c) and the thermal parts (P_{th}, ϵ_{th}). The cold parts are given by

$$P_c = K_1\rho^{\Gamma_1}, \quad \epsilon_c = \frac{K_1}{\Gamma_1 - 1}\rho^{\Gamma_1 - 1}, \qquad \text{as } \rho \leqslant \rho_{nuc},$$

$$P_c = K_2\rho^{\Gamma_2}, \quad \epsilon_c = \frac{K_2}{\Gamma_2 - 1}\rho^{\Gamma_2 - 1} + E_3, \quad \text{as } \rho > \rho_{nuc}, \tag{12}$$

with $K_1 = 4.9345 \times 10^{14}$ [cgs], while K_2 and E_3 are determined by the continuity of the pressure and energy density at $\rho = \rho_{nuc}$. The thermal parts that describe a mixture of non-relativistic and relativistic gases generate the pressure as $P_{th} = (\Gamma_{th} - 1)\rho\epsilon_{th}$. The nuclear matter EOS is determined by the three parameters $(\Gamma_1, \Gamma_2, \Gamma_{th})$, which are fixed to be $(1.3, 2.5, 1.35)$ by following reference [37].

Our numerical simulations for stellar core collapses are based on the open-source code GR1D [61], which was originally developed to model the spherically symmetric hydrodynamics in GR by exploying the high-resolution shock capturing scheme [64, 65]. The code was extended to include a massless scalar field in reference [43] and a massive one in references [44, 45], and was further implemented with an even-power scalar potential in references [46, 47]. Here we adopt all dynamical equations, grid types and boundary conditions in our simulations identical to those in reference [44].

3. Simulations and results

We focus on two specific progenitors of supernovae (pre-SN) with primordial metallicities of $M_{ZAMS} = 12M_\odot$ (denoted by WH12) and $M_{ZAMS} = 40M_\odot$ (denoted by WH40) from the catalog of realistic non-rotating pre-SN models of Woosley and Heger (WH) [66], respectively. In massive ST gravity [43], as well as in GR [67], it has been shown that WH12 will collapse

---

[7] After emanating from the inner core, the out-going shock will then be stalled by the inflowing material. If the shockwave successfully revives by some mechanisms, such as the standing accretion shock instability [56, 57], and the neutrino heating [58, 59], the explosion will be instigated and lead to a CCSNe. The mechanism that accounts for the revival is still an on-going problem (see, e.g. [60], for a recent review and the references therein).
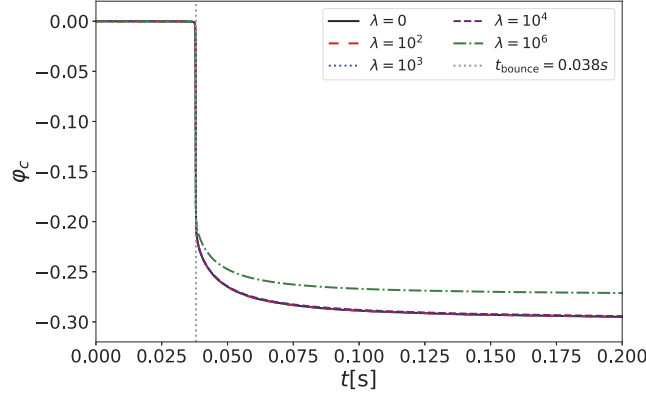
Figure 1. Evolutions of the central value of the scalar field φ_c during the core-collapse into an NS for the model WH12 with the self-interaction couplings of $\lambda = 0$, 10^2, 10^3, 10^4 and 10^6, respectively, where the vertical dashed line denotes the time of the stellar core bounce.

to form an NS remnant, while WH40 will eventually result in a BH after a stage of proto-NS (though see later).

The yet undermined ST parameters α_0 and β_0 in the conformal factor of equation (6) are chosen to allow strong scalarization in proto-NSs so as to generate significant scalar GW signals in our simulations. Their specific values will be given along with the detailed discussion of these two cases in section 3.1. Note that the initial value of the scalar field at every grid point is taken to be zero.

3.1. Numerical results on core collapse to neutron stars

For the particular progenitor WH12, the ST parameters are fixed to be $\alpha_0 = 10^{-2}$ and $\beta_0 = -20$, which trigger the strong scalarization in the remnant NS as shown in references [37, 44, 46]. Our main interest here is to investigate how the triple-scalar interaction in equation (7) affects the scalar field dynamics during the core collapse and its subsequently produced GW signals.

In figure 1, we show the scalar field value at the stellar center as a function of time, i.e. $\varphi_c(t) \equiv \varphi(t, r = 0)$. We can see that the strong spontaneous scalarization occurs at the time of the core bounce, $t \simeq 0.038$ s, for all triple-scalar coupling strength λ considered. The departure of the scalar dynamics around the star center from the non-interacting ST gravity ($\lambda = 0$) is found to be inconsiderable for a moderate coupling strength $\lambda \lesssim 10^4$. However, when λ approaches or exceeds $\sim 10^6$, we can observe the significant suppression in the magnitude of the scalarization (the green dashed line in figure 1).

The suppression of the spontaneous scalarization is more evident in the rescaled field

$$\sigma \equiv r\varphi. \tag{13}$$

According to its definition, the leading-order term of σ reduces to the scalar charge χ in the massless ST gravity [43], which is defined as the coefficient of the $1/r$ term in the asymptotic behavior of the scalar field at spatial infinity, i.e.

$$\varphi = \frac{\chi}{r} + O(r^{-2}). \tag{14}$$
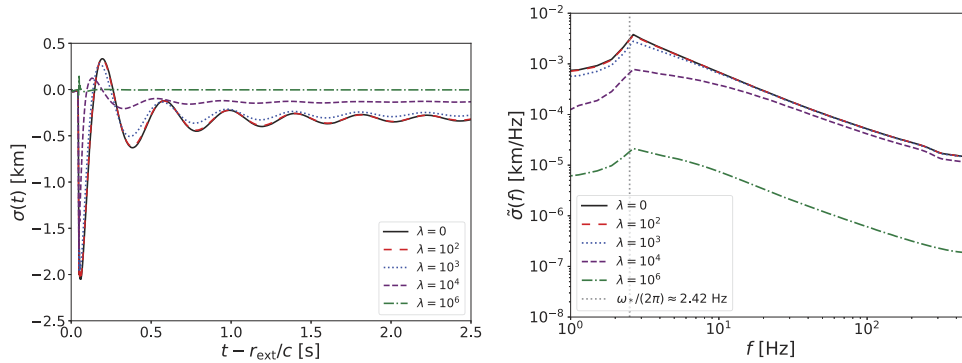
Figure 2. Scalar GW signals for WH12 extracted at the radius $r_{ex} = 5 \times 10^4$ km for the self-interaction couplings of $\lambda = 0$, 10^2, 10^3, 10^4 and 10^6, respectively, where the vertical line on the right plot denotes the characteristic frequency $f_* = 2.42$ Hz.

Extracting σ at a fixed distance of $r_{ex} = 5 \times 10^4$ km, in figure 2 we plot $\sigma_{ex} \equiv \sigma(r_{ex})$ in the time domain (left panel), and the associated Fourier transformed signals $\tilde{\sigma}_{ex}(f)$ [68] in the frequency domain (right panel). For the self-coupling up to $\lambda \sim 10^2$, the difference in σ_{ex} from the non-self-interacting ST gravity is negligible. However, when λ approaches $\sim 10^3$, we begin to see a mild suppression and a small phase shift. The suppression and the phase shift are enlarged with increasing λ as a consequence of the frequency-related suppression caused by the scalar self-interaction (similar to the fashion of reference [46]). Finally, when $\lambda \gtrsim 10^6$, the scalarization is reduced from the case without the self-interaction by more than two orders.

In addition, the frequency-domain plot (the right panel of figure 2) shows that the suppression is more significant for $f \lesssim f_* = 2.42$ Hz. Due to their smaller group velocities, the low-frequency modes spend more time propagating out of the (strong) interaction regime near the star so that they experience more suppressions by self-interactions. To illustrate this effect, we plot σ at three radii $r_{ex} = (5, 10, 15) \times 10^4$ km with $\lambda = 10^3$ in figure 3. These distances lie in the wave zone [45] and are much larger than both the reduced Compton wavelength of the massive scalar $\lambda_C = c/(2\pi f_*)$ and the gravitational radius $r_G = GM_{NS}/c^2$ with M_{NS} denoting the NS mass. In the left panel of figure 3, we see that the time-domain signal becomes much more oscillatory since the dispersion during the propagation screens out the low frequency modes for a distant observer, as expected. When transformed into the frequency domain (the right panel of figure 3), the modes with frequencies higher than f_* remain unchanged, while the spectra below this critical frequency decay exponentially. This implies that only the high-frequency scalar signals can travel astrophysically long distance to be detectable on the Earth. Focusing on the high frequency signals, the choice of the extraction radius is irrelevant therefore.

3.2. Numerical results on core collapse to black holes

Now we turn to simulation results for the progenitor model WH40. In order for the strong scalarization to occur in the proto-NS prior to the BH formation, we set the ST parameters as $\alpha_0 = 3 \times 10^{-3}$ and $\beta_0 = -5$. We shall repeat the above analysis to see the effects of the self-interaction term in equation (7) on the dynamics of the stellar evolution and the scalar-polarized GW radiations.

Figure 4 presents the evolutions of the scalar field at the center of the compact objects for the WH40 progenitor. Obviously, the dynamics is much more complicated than the WH12 model. We begin our discussion with the non-self-interacting case, i.e. $\lambda = 0$. The stellar core bounce
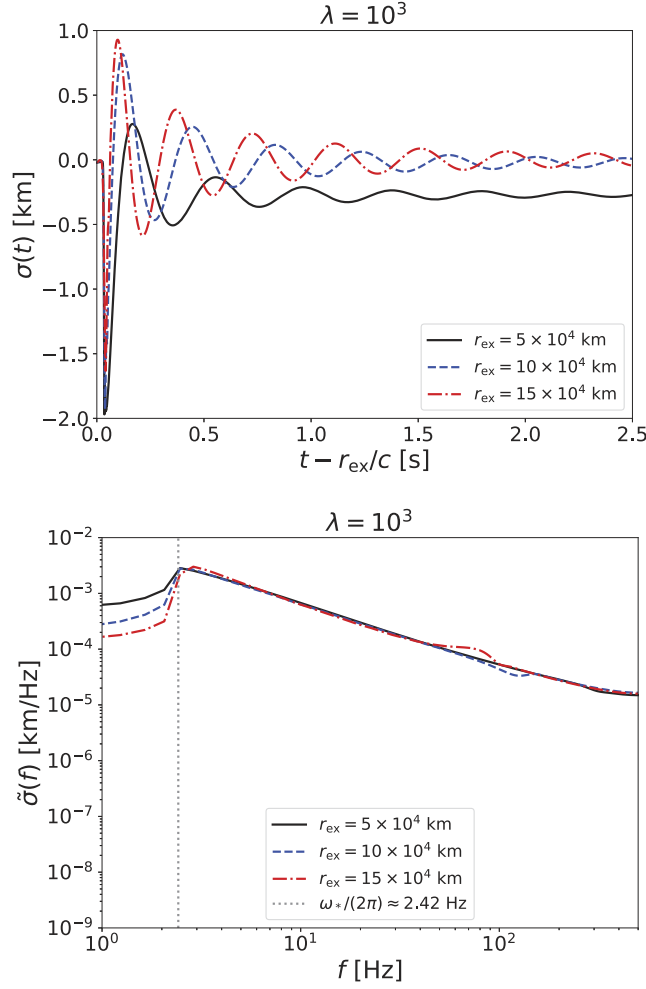
Figure 3. Scalar GW waveforms for WH12 extracted at different radii $r_{\text{ex}} = (5, 10, 15) \times 10^4$ km.

firstly produces a weakly scalarized NS with $\varphi_c \sim -5 \times 10^{-4}$ at $t_w \simeq 0.085$ s, which then transits to a strongly scalarized NS at $t_s \simeq 0.35$ s due to the accretion of ambient materials. In this particular model, the continuous infalling material makes the stellar core massive enough to cause the gravitational instability, i.e. the mass of the remnant exceeds the maximal mass that can be supported by the EOS considered. Eventually, a BH forms at some point t_{BH}, which depends on λ (see below).

The extent to which the scalarization is triggered and the lifetime of the strongly-scalarized state ($t_{\text{BH}} - t_s$) depend on λ. The left panel of figure 4 shows the cases with a moderate level of λ, where we see that φ_c goes down to ~ -0.25 at t_s, and then the scalarization is progressively strengthened to $\varphi_c \sim -0.35$ at the moment right before the BH formation. The strong scalarization lasts for ~ 1.24 s, and is followed by a transient decrease of the scalarization at t_{BH} in accordance with the BH no-hair theorem. In addition, when $\lambda \lesssim 10^3$, we do not see any visible deviation from the case without self-interactions. As λ increases to $\gtrsim 10^4$, the degree of the scalarization during the strong-scalarization stage is weakened a little, but the duration
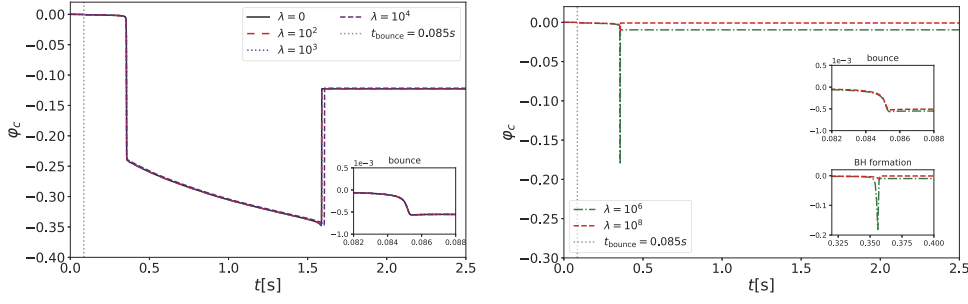
Figure 4. Evolutions of the central value of the scalar field φ_c for the progenitor WH40 during the core-collapse into a BH for $\lambda = 0$, 10^2, 10^3 and 10^4 in the left panel and $\lambda = 10^6$ and 10^8 in the right panel, respectively, where the inset of left panel shows the scalar field behavior zoomed in on the core bounce part, while ones on the right panel correspond to the region near the core bounce and the BH formation, respectively.

$t_{BH} - t_s$ becomes a bit longer owing to a delay in the BH formation. Such trend continues and becomes more evident with increasing λ until $\lambda \sim 10^6$. In the right panel of figure 4, we plot the case with strong coupling strengths $\lambda = 10^6$ and 10^8. For $\lambda = 10^6$, the degree of the scalarization is a bit slighter than the aforementioned case with the moderate λ and the lifetime of the proto-NS becomes very short with $t_{BH} - t_s \lesssim 0.01$ s. When $\lambda = 10^8$, we find that the strongly-scalarized proto-NS stage completely disappears, leading to a scenario that a weakly-scalarized NS directly collapses to a BH.

Having shown the influence of λ on φ_c, we now turn to investigate how λ affects σ, especially σ_{ex}. In figures 5 and 6, we present σ_{ex} in both the time and the frequency domains. As illustrated in the left panel of figure 5, we can find clear time-domain signatures corresponding to the transitions between different stages of the multi-stage BH formation scenario. In the inset figure, we see a small variation in the amplitude at the retarded time $t_r \equiv t - r_{ex}/c = 0.085$ s, which matches the timing of the core bounce. The sudden drop at $t_r \simeq 0.35$ s and the sharp peak around $t_r \simeq 1.59$ s reflect the transition from weakly- to strongly-scalarized configurations and the descalarization caused by the BH formation. Moreover, compared with the non-self-interacting case, the evolution of σ_{ex} keeps intact for $\lambda \lesssim 10^3$. When λ increases to 10^4, the suppression of the amplitude for GW signals can be seen in both the time and frequency domains. On the other hand, as shown in the left panel of figure 6, besides the small structure at the core bounce, we only see some rapid oscillations around the BH formation for $\lambda \gtrsim 10^6$, which indicates the disappearance of the strongly-scalarized NS stage. Furthermore, the right panel of figure 6 illustrates that the scalarization is diminished greatly by several orders for $\lambda = 10^6$ and 10^8 in comparison with the case of $\lambda = 0$.

4. Scalar GW propagation and its detectability
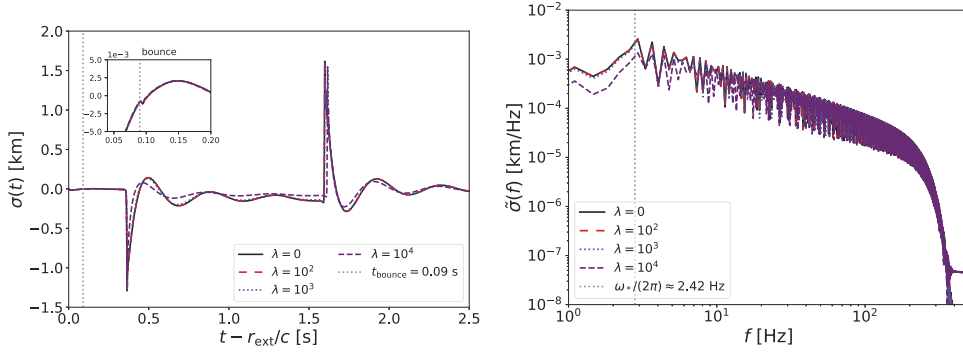
4.1. Scalar GW signals

In the ST gravity, the scalarization contributes the strain amplitude [3, 70]:

$$h_s = h_B - h_L, \tag{15}$$

to the GW signal of the angular frequency Ω, where

$$h_B = 2\alpha_0\varphi, \tag{16}$$

Figure 5. Scalar GW signals in the time domain (left panel) and frequency domain (right panel) for the progenitor model WH40 extracted at the radius $r_{ex} = 5 \times 10^4$ km for different values of the self-interaction coupling $\lambda = 0$, 10^2, 10^3 and 10^4, respectively. The inset in the left panel illustrates the scalar GWs around the core bounce which generates a weakly-scalarized NS.
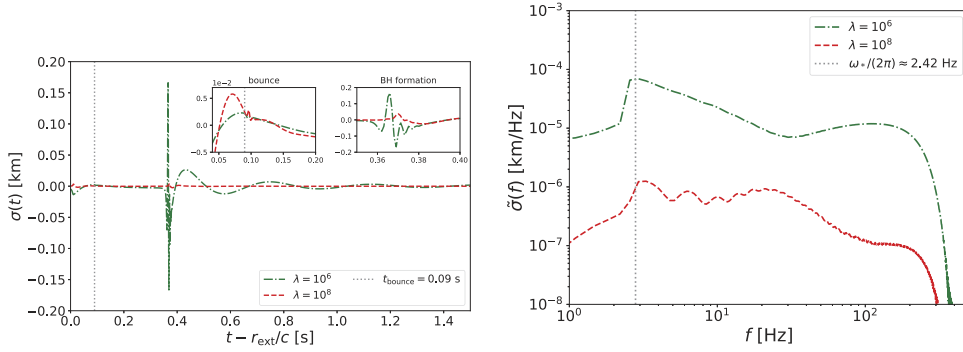
Figure 6. Label is the same as figure, except for $\lambda = 10^6$ and 10^8. The two insets in the left panel correspond to the scalar GW signals at the core bounce and the BH formation, where we have artificially enlarged the field values by a factor of 10 for the case with $\lambda = 10^8$ in order to make its dynamical evolution clearer.

is the so-called breathing mode which is transverse and scalar-polarized, and

$$h_{\mathrm{L}} = \left(\frac{\omega_*}{\Omega}\right)^2 h_{\mathrm{B}} = 2\alpha_0 \left(\frac{\omega_*}{\Omega}\right)^2 \varphi, \tag{17}$$

is the longitudinally polarized mode, respectively. For a GW interferometer, the detector responses to the scalarization-induced GW strain through

$$h(t) = F_\circ[\theta(t), \phi(t)]h_{\mathrm{s}}(t), \tag{18}$$

where $F_\circ \equiv -\sin^2\theta \, \cos 2\phi/2$ is the interferometer antenna pattern [3, 71] which depends on the sky location (θ, ϕ) of the source in the internal frame of the detector. Note that these two scalar polarizations share the identical antenna pattern function up to a sign [3, 70], so that they cannot be distinguished experimentally. For simplicity, we take the sky averaged rms value of

the antenna pattern function [45]

$$\bar{F}_\circ = \sqrt{\iint d\theta\, d\phi\, \sin\theta F^2(\theta,\phi)} = \sqrt{4\pi/15} \tag{19}$$

as the canonical value.

Currently, in order for the highly scalarized NSs to evade the strong constraints from the observation of the orbital decay of binary pulsars such as the pulsar-white dwarf system PSR J0348 + 0432 [29], we need to impose a lower limit on the scalar mass as $\mu > \mathcal{O}(10^{-15})$ eV [31, 32], corresponding to a lower frequency bound of $\mathcal{O}(0.1$ Hz) via equation (8). The GW modes above this bound lies in the sensitive range of ground-based GW detectors, such as LIGO-Virgo [72–74], Cosmic Explorer (CE) [75] and Einstein Telescope (ET) [76]. In the literature, the detectability of the GW signal in equation (15) for a single detector is characterized by the corresponding SNR which is defined as follows [77]:

$$\rho^2 = 4\int_0^\infty df \frac{|\tilde{h}(f)|^2}{S_n(f)}, \tag{20}$$

where $\tilde{h}(f)$ denotes the Fourier transformed function of the response in equation (18), while $S_n(f)$ is the one-sided noise power spectral density of the instrument given by the corresponding experimental collaboration.

4.2. Scalar GW propagation

After the scalar GWs (equation (15)) are generated from the stellar core-collapse in our Galaxy, they propagate over an astronomically long distance of $\mathcal{O}(10$ kpc) before they are detected on the Earth. According to the action in equation (4), the propagation of the scalar GW far away from its source can be well approximated by the wave equation in the nearly flat space:

$$\begin{cases} \dfrac{\partial^2\sigma}{\partial t^2} - \dfrac{\partial^2\sigma}{\partial r^2} + \dfrac{\mu^2}{\hbar^2}\sigma + \dfrac{3\lambda\mu^2}{2\hbar^2}\dfrac{\sigma^2}{r} = 0, & \text{as } \sigma \geqslant 0, \\[2ex] \dfrac{\partial^2\sigma}{\partial t^2} - \dfrac{\partial^2\sigma}{\partial r^2} + \dfrac{\mu^2}{\hbar^2}\sigma - \dfrac{3\lambda\mu^2}{2\hbar^2}\dfrac{\sigma^2}{r} = 0, & \text{as } \sigma < 0, \end{cases} \tag{21}$$

where the equation is written in the spherically symmetric coordinate with $\sigma \equiv r\varphi$. The interaction term drops faster than the mass term by one power of r, and the mass term will dominate after a certain distance. The subsequent long-distance propagation is thus barely affected by the self-interactions. In this case, the description of the scalar GWs can be further reduced to the following wave equation without interactions

$$\frac{\partial^2\sigma}{\partial t^2} - \frac{\partial^2\sigma}{\partial r^2} + \frac{\mu^2}{\hbar^2}\sigma = 0, \quad \text{as } r \to \infty. \tag{22}$$

From this simplified equation, we can obtain the asymptotic behavior of the scalar field. Concretely, when the frequency is below the critical one $f_* = \omega/(2\pi) \equiv \mu/(2\pi\hbar) \simeq 2.42$ Hz, the mode damps as the Yukawa-like suppression where $\varphi \sim e^{-\kappa r}/r$ with $\kappa = \sqrt{\mu^2 - \omega^2}$. In fact, we have already seen this suppression from the frequency spectra of the scalar GW at different extraction distances on the right plot of figure 3, in which the GW amplitudes of the modes with frequencies below the critical one decrease aggressively when the extraction radius becomes distant. On the other hand, when the frequency is above the critical one, the mode becomes a propagating out-going wave as $\varphi \sim e^{ikr}/r$. In this case, the wavelength is predicted to be

$k = \sqrt{\omega^2 - \mu^2}$. Since these modes can approach the spatial infinity, we can define the scalar charge χ as the massless scalar case, just like in equation (14).

As pointed out in references [44, 45], due to the presence of the mass term, the GW signal becomes more and more oscillatory with time. The dispersive nature of the propagation introduces tremendous difficulties in the numerical calculations of the GW evolution in space. In the present work, we adopt the stationary phase approximation (SPA) [69] to evaluate the scalar GW waveform at large radii. The scalar GW signal at r_{ex} can be expanded by the Fourier series, in which the component with frequency ω reads

$$\tilde{\sigma}(\omega; r_{\text{ex}}) = \mathcal{A}(\omega; r_{\text{ex}})e^{i\Psi(\omega)}, \tag{23}$$

where $\mathcal{A}(\omega; r_{\text{ex}})$ and $\Psi(\omega)$ are the scalar wave amplitude and phase, respectively. In the limit of $r \gg r_{\text{ex}}$, the scalar GW signal is highly dispersive and becomes quasi-monochromatic at the frequency

$$\Omega(t) = \frac{\omega_* t}{\sqrt{t^2 - (r - r_{\text{ex}})^2}}, \quad \text{for } t > r - r_{\text{ex}}. \tag{24}$$

Note that this frequency shows the signature of the inverse chirp [44], which means that high-frequency modes arrive earlier than low-frequency (but still higher than ω_*) ones. Such a feature is originated from the fact that scalar GW modes with higher frequencies have larger group velocities, and thus reach us with less time. Furthermore, the SPA method also gives the following amplitude of the scalar GW at a large radii r [44, 45]

$$A(\Omega; r) = \sqrt{\frac{2[\Omega^2 - \omega_*^2]^{3/2}}{\pi \omega_*^2 (r - r_{\text{ex}})}} \mathcal{A}(\Omega; r_{\text{ex}}), \tag{25}$$

in which the frequency Ω is a function of time t given by equation (24).

As argued in reference [45], for a (quasi-)monochromatic scalar GW signal, the SNR equation (20) can be estimated as follows

$$\rho \approx \sqrt{\frac{S_o(f)}{S_n(f)}}. \tag{26}$$

Here, the spectral power density of the GW signal is given by

$$\sqrt{S_o(f)} = \sqrt{T} \alpha_0 \bar{F}_\circ \left(\frac{A(2\pi f; D)}{D} \right) \left[1 - \left(\frac{\omega_*}{\Omega} \right)^2 \right], \tag{27}$$

where D is the distance between the star and the Earth, while T denotes the duration of the observation.

4.3. Scalar GW detectability

For the scalar GW signals in the ST gravity, there exist several search strategies [44], such as monochromatic continuous-wave searches, stochastic searches, and burst searches. Note that the observable scalar GW signal in the massive ST theory is nearly monochromatic, even though the waveform near the source is not at all. This universal feature is caused by the scalar mass term μ which would make the scalar GW signal highly dispersed. Concretely, by inspecting the simplified equation of motion in equation (22), it is obvious that different frequency

modes have distinct group velocities

$$v_g = \frac{\mathrm{d}\omega}{\mathrm{d}k} = \sqrt{1 - \left(\frac{\omega_*}{\omega}\right)^2}, \tag{28}$$

where $\omega_* \equiv \mu/\hbar$. Moreover, as the frequency approaches to the critical one, the mode group velocity becomes extremely small. This fact indicates that, no matter what the original GW waveform is, after the propagation along an astronomical distance, the signal would be distorted into the one in which modes with the higher frequencies would reach the detector at the Earth much earlier than those with lower frequencies, which is just the inverse chirp phenomenon [44] dictated by equation (24). Moreover, since the propagation distance is astronomically long, the signal would last for several decades or even centuries, and the time lag between different frequency modes would be highly enhanced. As a result, the signal at the detector would be quasi-monochromatic with the frequency evolution extremely slow. Typically, for a signal 10 years after its first detection by the optical observation of a supernova explosion, we need to wait for several months to see the variation of its frequency under the current detection precision. Therefore, for a core-collapse supernova that is possibly detected by optical observations or all-sky GW searches, the best strategy is through the continuous quasi-monochromatic GW search [44, 45, 47] pointed to the location of that source, which was originally proposed to detect the GWs from spinning neutron stars and axion clouds [78]. In this subsection, we present our prediction of the detectabilities of such source-targeted continuous searches of the scalar GW signals for the progenitor models WH12 and WH40.

By employing the scalar GW waveforms extracted at $r_{\mathrm{ex}} = 5 \times 10^4$ km to equation (27), we can obtain the spectral power densities for both progenitor models. In figure 7, we plot $\sqrt{S_o(f)}$ at several time points after the GW emission with various triple-scalar coupling strengths. Here, the distance between the Earth and the source is assumed to be of the galactic scale, i.e. $D = 10$ kpc. Since the signal would keep nearly monochromatic for the period of $\mathcal{O}$ (month), the observational duration is taken to be $T = 2$ months. For both WH12 and WH40, we can see that (i) the quasi-monochromatic signal slowly moves to low frequencies in accord with the inverse-chirp formula in equation (24), (ii) $\sqrt{S_o(f)}$ varies within two orders over time for a given coupling strength, and (iii) the triple-scalar self-interaction suppresses the magnitude of the scalar gravitational radiation generated by the stellar core collapses. The predicted scalar GW signals are similar to the non-interacting case for up to $\lambda \sim 10^3$, whereas we observe a small reduction in the signal amplitude when λ increases to $\sim 10^4$. When $\lambda \gtrsim 10^6$, the scalar-polarized GW is suppressed by two orders for the WH12 model, while for the WH40 progenitor the suppression is frequency-dependent, viz the low-frequency modes decrease in amplitude more than the high-frequency part of the spectrum.

On top of the scalar GW strain of our models, figure 7 also shows the noise curves of the current LIGO detectors, and the near-future ET and CE experiments, whereby we can estimate the SNRs of signals. It turns out that, even though the scalar GW signal amplitude of the WH12 model with $\lambda \lesssim 10^4$ observed for 2 months in the first 3 years after the core collapse can be higher than the LIGO noise curve, the SNR in this optimal case can only reach $\rho \simeq 2$ at most, which is unlikely to be detected. For other choices of the coupling constant values, progenitor models and detection times would result in power spectral densities $\sqrt{S_o}$ lower than the LIGO sensitivity curve, implying that it is impossible to measure them with LIGO. In contrast, with the future ET and CE detectors, some signals may reach SNRs of $\rho \sim \mathcal{O}(100)$ and remains visible for several centuries.
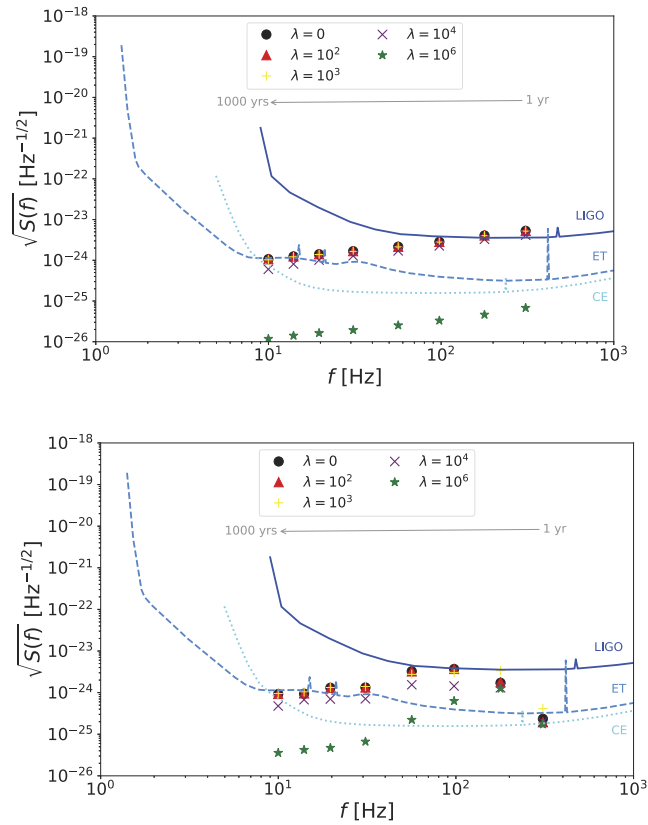
Figure 7. Power spectrum densities of the core collapse into an NS for the progenitor models WH12 (upper panel) and into a BH for WH40 (lower panel) with the self-interaction couplings $\lambda = 0$, 10^2, 10^3, 10^4 and 10^6, respectively, where the points of various types correspond to the inverse-chirp scalar GW signals observed at different times after the supernova: $t = 1, 3, 10, 30, 100, 250, 500$, and 1000 years from right to left on each plot. In comparison, we also plot the noise power spectral density of LIGO, ET, and CE.

5. Conclusions and discussions

The stellar core collapse provides us with valuable tests of ST theories due to the possible formation of the NS in the intermediate stage or as the final state of the process. The spontaneous scalarization may be induced in those NS and produces strong scalar or monopole GW signals. In the present work, we have studied the effects of the triple-scalar self-interaction defined in equation (7) on the scalar field dynamics and the subsequent scalar GW generation. In order to achieve this goal, we have performed simulations based on the open-source code GR1D which is extended to the massive ST gravity with the triple-scalar self-interaction. We have focused on two specific pre-SN models with the primordial metallicity in the WH list, viz WH12 and WH40, corresponding to stars with ZAMS mass of $12M_\odot$ and $40M_\odot$, respectively. These two progenitors are representative of two typical collapse processes; WH12 collapses into an NS, while WH40 ends up to a BH. The ST parameters α_0 and β_0 are chosen specifically for each model so that the strong scalarization can take place in simulations.

As a result, we have found that the triple-scalar self-interaction can generically suppress the degree of the scalarization during the collapse, which is consistent with the conclusions in references [46, 47]. Such suppressions can be shown either from the scalar dynamics at the center of the star or from the produced scalar GW signals. Furthermore, the suppression is considerable only when the self-interaction coupling λ becomes sufficiently large, i.e. $\lambda \gtrsim 10^3$ for WH12 and $\lambda \gtrsim 10^4$ for WH40. More interestingly, the self-interaction can even alter the scalar evolutionary history of the collapse for the WH40 model by completely eliminating the strongly scalarized stage during the BH formation as λ reaches a critical value of $\mathcal{O}(10^6)$.

For the massive scalar GWs propagate over astrophysically long distances, the self-interaction effects have been shown to be negligible, and the dispersion of GWs is solely determined by the scalar mass. It turns out that scalar GW signals detected on the Earth have the inverse-chirp feature as that have been suggested by massive ST theories without self-interactions [37, 44]. We have accessed the detectability of the scalar GW signals produced by the galactic WH12 and WH40 pre-SN sources by estimating their SNRs. Although it is unlikely to observe the inverse-chirp signals for both progenitors with the current LIGO detectors, signals of these two models can reach SNRs of $\mathcal{O}(100)$ with the future ET and CE detectors and remain visible for several centuries.

In this study, our simulations have been performed with fixed nuclear matter EOS parameters and specific values of the ST gravity parameters (α_0, β_0). However, it is well known that the nuclear matter property would significantly affect the hydrodynamic evolution of matter fields during the core collapse [79, 80], which would in turn dramatically modify the dynamics of the scalar field and the generated GW waveforms. Additionally, it has been pointed out in reference [45] that the stellar collapse scenarios changes with the different choices of the ST parameters (α_0, β_0). Especially, as the value of β_0 becomes more and more negative, the degree of scalarization tends to be intensified and the corresponding GW signals are expected to be stronger. Moreover, there have been several studies on the spectrum of radial quasinormal modes (QNMs) of NSs in the ST gravity theory [81–83]. It is well expected that the radial QNMs would show themselves in the scalar GW spectrum at the late stage of the stellar collapse. According to the discussion in reference [81] which has also addressed the spontaneously scalarized NSs with a negative β_0, there are two classes of radial QNMs: the pressure-led fluid modes and the scalar ϕ-modes. It is seen from the plots of figure 2 in this reference that typical frequencies of the fluid modes are of $\mathcal{O}$ (kHz) and that of the fundamental ϕ-mode is around or below 1 kHz, while the damping times of these modes are of $\mathcal{O}(0.1 - 1)$ ms. However, in our simulation, the minimal sampling time interval is only 1 ms, which means that we do not have enough precision to resolve the QNM signals for both modes. In order to see these modes clearly, one needs to improve the simulation precision in time interval at least by one to two orders. Nevertheless, the full exploration of all these aspects is well beyond the scope of the present article, and will be deferred to the future work.

Acknowledgments

Data availability statement

All data that support the findings of this study are included within the article (and any supplementary files).

ORCID iDs

Da Huang ⬤ https://orcid.org/0000-0001-8357-754X
Chao-Qiang Geng ⬤ https://orcid.org/0000-0002-7303-4581
Hao-Jui Kuan ⬤ https://orcid.org/0000-0002-3480-3448

References

[1] Psaltis D 2008 *Living Rev. Relativ.* **11** 9
[2] Berti E *et al* 2015 *Class. Quantum Grav.* **32** 243001
[3] Will C M 2014 *Living Rev. Relativ.* **17** 4
[4] Abbott B P *et al* (LIGO Scientific and Virgo Collaboration) 2016 *Phys. Rev. Lett.* **116** 221101
     Abbott B P *et al* (LIGO Scientific and Virgo Collaboration) 2018 *Phys. Rev. Lett.* **121** 129902 erratum
[5] Burgess C P 2004 *Living Rev. Relativ.* **7** 5–56
[6] Spergel D N 2015 *Science* **347** 1100–2
[7] Jordan P 1959 *Z. Phys.* **157** 112–21
[8] Fierz M 1956 *Helv. Phys. Acta* **29** 128–34 http://retro.seals.ch/digbib/view2?pid=hpa-001:1956:29::132
[9] Brans C and Dicke R H 1961 *Phys. Rev.* **124** 925–35
[10] Salgado M 2006 *Class. Quantum Grav.* **23** 4719–41
[11] Salgado M, Martinez-del Rio D, Alcubierre M and Núñez D 2008 *Phys. Rev. D* **77** 104010
[12] Damour T and Esposito-Farese G 1992 *Class. Quantum Grav.* **9** 2093–176
[13] Chiba T, Harada T and Nakao K-i 1997 *Prog. Theor. Phys. Suppl.* **128** 335–72
[14] Fujii Y and Maeda K 2007 *The Scalar–Tensor Theory of Gravitation* (Cambridge: Cambridge University Press)
[15] Faraoni V 2004 *Cosmology in Scalar Tensor Gravity* (Berlin: Springer) https://doi.org/10.1007/978-1-4020-1989-0
[16] Sotiriou T P 2015 *Lect. Notes Phys.* **892** 3–24
[17] Dai D-C and Stojkovic D 2019 *Class. Quantum Grav.* **36** 145004
[18] Akbarieh A R, Kazempour S and Shao L 2021 *Phys. Rev. D* **103** 123518
[19] Shapiro I I 1999 *Rev. Mod. Phys.* **71** S41–53
[20] Williams J G, Turyshev S G and Boggs D H 2009 *Int. J. Mod. Phys. D* **18** 1129–75
[21] Shapiro S S, Davis J L, Lebach D E and Gregory J S 2004 *Phys. Rev. Lett.* **92** 121101
[22] Bertotti B, Iess L and Tortora P 2003 *Nature* **425** 374–6
[23] Ventagli G, Lehébel A and Sotiriou T P 2020 *Phys. Rev. D* **102** 024050
[24] Salgado M, Sudarsky D and Nucamendi U 1998 *Phys. Rev. D* **58** 124003
[25] Damour T and Esposito-Farèse G 1993 *Phys. Rev. Lett.* **70** 2220–3
[26] Damour T and Esposito-Farèse G 1996 *Phys. Rev. D* **54** 1474–91
[27] Wex N 2014 arXiv:1402.5594 [gr-qc]
[28] Freire P C C *et al* 2012 *Mon. Not. R. Astron. Soc.* **423** 3328
[29] Antoniadis J *et al* 2013 *Science* **340** 6131
[30] Shao L, Sennett N, Buonanno A, Kramer M and Wex N 2017 *Phys. Rev. X* **7** 041025
[31] Ramazanoğlu F M and Pretorius F 2016 *Phys. Rev. D* **93** 064005
[32] Morisaki S and Suyama T 2017 *Phys. Rev. D* **96** 084026
[33] Xu R, Gao Y and Shao L 2020 *Phys. Rev. D* **102** 064057
[34] Yunes N, Yagi K and Pretorius F 2016 *Phys. Rev. D* **94** 084002
[35] Abbott B P *et al* (LIGO Scientific and Virgo Collaboration) 2019 *Phys. Rev. Lett.* **123** 011102
[36] Abbott B P *et al* (LIGO Scientific and Virgo Collaboration) 2019 *Phys. Rev. D* **100** 104036

[37] Geng C-Q, Kuan H-J and Luo L-W 2020 *Eur. Phys. J.* C **80** 780
[38] Geng C-Q, Kuan H-J and Luo L-W 2020 *Class. Quantum Grav.* **37** 115001
[39] Andreou N, Franchini N, Ventagli G and Sotiriou T P 2019 *Phys. Rev.* D **99** 124022
     Andreou N, Franchini N, Ventagli G and Sotiriou T P 2020 *Phys. Rev.* D **101** 109903 erratum
[40] Novak J 1998 *Phys. Rev.* D **57** 4789–801
[41] Novak J 1998 *Phys. Rev.* D **58** 064019
[42] Novak J and Ibanez J M 2000 *Astrophys. J.* **533** 392–405
[43] Gerosa D, Sperhake U and Ott C D 2016 *Class. Quantum Grav.* **33** 135002
[44] Sperhake U, Moore C J, Rosca R, Agathos M, Gerosa D and Ott C D 2017 *Phys. Rev. Lett.* **119** 201103
[45] Rosca-Mead R, Sperhake U, Moore C J, Agathos M, Gerosa D and Ott C D 2020 *Phys. Rev.* D **102** 044010
[46] Cheong P C K and Li T G F 2019 *Phys. Rev.* D **100** 024027
[47] Rosca-Mead R, Moore C J, Agathos M and Sperhake U 2019 *Class. Quantum Grav.* **36** 134003
[48] Bergmann P G 1968 *Int. J. Theor. Phys.* **1** 25–36
[49] Wagoner R V 1970 *Phys. Rev.* D **1** 3209–16
[50] Bardeen J M 1983 *Gravitational Radiation* ed T Deruelle and N Piran (Amsterdam: North-Holland) pp 433–41
[51] O'Connor E and Ott C D 2011 *Astrophys. J.* **730** 70
[52] Clausen D, Piro A L and Ott C D 2015 *Astrophys. J.* **799** 190
[53] Sukhbold T, Ertl T, Woosley S E, Brown J M and Janka H T 2016 *Astrophys. J.* **821** 38
[54] Bethe H A 1990 *Rev. Mod. Phys.* **62** 801–66
[55] Dimmelmeier H, Font J A and Müller E 2002 *Astron. Astrophys.* **393** 523–42
[56] Burrows A, Livne E, Dessart L, Ott C and Murphy J 2006 *Astrophys. J.* **640** 878–90
[57] Harada A, Nagakura H, Iwakami W and Yamada S 2017 *Astrophys. J.* **839** 28
[58] Janka H-T 2001 *Astron. Astrophys.* **368** 527
[59] Pejcha O and Thompson T A 2012 *Astron. Astrophys.* **746** 106
[60] Couch S M 2017 *Phil. Trans. R. Soc.* A **375** 20160271
[61] O'Connor E and Ott C D 2010 *Class. Quantum Grav.* **27** 114103
[62] Janka H T, Zwerger T and Moenchmeyer R 1993 *Astron. Astrophys.* **268** 360–8
[63] Zwerger T and Mueller E 1997 *Astron. Astrophys.* **320** 209–27
[64] Font J A, Miller M A, Suen W M and Tobias M 2000 *Phys. Rev.* D **61** 044011
[65] Font J A 2008 *Living Rev. Relativ.* **11** 7
[66] Woosley S and Heger A 2007 *Phys. Rep.* **442** 269–83
[67] Kuan H J, Doneva D D and Yazadjiev S S 2021 arXiv:2103.11999 [gr-qc]
[68] Ivezic Z, Connolly A, VanderPlas J and Gray A 2013 *Statistics, Data Mining, and Machine Learning in Astronomy* (Princeton, NJ: Princeton University Press)
[69] Bender C and Orszag S 1978 *Advanced Mathematical Methods for Scientists and Engineers* (New York: McGraw-Hill)
[70] Will C M 1994 *Phys. Rev.* D **50** 6058–67
[71] Babusci D, Baiotti L, Fucito F and Nagar A 2001 *Phys. Rev.* D **64** 062001
[72] Aasi J *et al* (LIGO Scientific Collaboration) 2015 *Class. Quantum Grav.* **32** 074001
[73] Acernese F *et al* (VIRGO Collaboration) 2015 *Class. Quantum Grav.* **32** 024001
[74] Abbott B P *et al* (KAGRA, LIGO Scientific and VIRGO Collaboration) 2018 *Living Rev. Relativ.* **21** 3
[75] Abbott B P *et al* (LIGO Scientific Collaboration) 2017 *Class. Quantum Grav.* **34** 044001
[76] Punturo M *et al* 2010 *Class. Quantum Grav.* **27** 194002
[77] Moore C J, Cole R H and Berry C P L 2015 *Class. Quantum Grav.* **32** 015014
[78] Riles K 2017 *Mod. Phys. Lett.* A **32** 1730035
[79] Dimmelmeier H, Ott C D, Janka H-T, Marek A and Müller E 2007 *Phys. Rev. Lett.* **98** 251101
[80] Dimmelmeier H, Ott C D, Marek A and Janka H T 2008 *Phys. Rev.* D **78** 064056
[81] Mendes R F P and Ortiz N 2018 *Phys. Rev. Lett.* **120** 201104
[82] Blázquez-Salcedo J L, Scen Khoo F and Kunz J 2020 *Europhys. Lett.* **130** 50002
[83] Blázquez-Salcedo J L, Khoo F S, Kunz J and Preut V 2021 *Front. Phys.* **9** 484